PNAS RESEARCH ARTICLE | APPLIED PHYSICAL SCIENCES

Statistics and topology of fluctuating ribbons

Ee Hou Yong[a,1], Farisan Dary[a], Luca Giomi[b], and L. Mahadevan[c,d,e,1]

Edited by Frederick MacKintosh, Rice University, Houston, TX; received December 19, 2021; accepted April 26, 2022 by Editorial Board Member Daan Frenkel

Ribbons are a class of slender structures whose length, width, and thickness are widely separated from each other. This scale separation gives a ribbon unusual mechanical properties in athermal macroscopic settings, for example, it can bend without twisting, but cannot twist without bending. Given the ubiquity of ribbon-like biopolymers in biology and chemistry, here we study the statistical mechanics of microscopic inextensible, fluctuating ribbons loaded by forces and torques. We show that these ribbons exhibit a range of topologically and geometrically complex morphologies exemplified by three phases—a twist-dominated helical phase (HT), a writhe-dominated helical phase (HW), and an entangled phase—that arise as the applied torque and force are varied. Furthermore, the transition from HW to HT phases is characterized by the spontaneous breaking of parity symmetry and the disappearance of perversions (that correspond to chirality-reversing localized defects). This leads to a universal response curve of a topological quantity, the link, as a function of the applied torque that is similar to magnetization curves in second-order phase transitions.

statistical mechanics | polymer physics | topological mechanics

Significance

Microscopic ribbons are ubiquitous in nature, and common examples include α helices, β sheet, graphene nanoribbons, etc. Yet their response to external loads is still largely unknown, especially when accounting for thermal effects that dominate on small scales. We characterize the rich morphological phase diagram that spans the torque–force–temperature phase space of microscopic ribbons, using numerical simulations and analysis, leading to a set of experimentally testable predictions for the statistics of fluctuating ribbons that are qualitatively different from those of the well-studied worm-like chain model of stiff polymers.

Filamentous structures are ubiquitous in molecular and cellular biology, polymer chemistry, and physics (1–3). These structures are characterized by their geometrical scale separation, whereby one length scale (the length) is very large compared to the other two (the two principal radii), with consequences for their mechanical properties, for example, they are easy to bend and twist and hard to stretch and shear. In addition, when the smallest of these scales is comparable to a characteristic length $\ell \approx (k_B T/G)^{1/3}$ obtained by balancing the energy associated with thermal fluctuations $k_B T$ (k_B is the Boltzmann constant, and T is the absolute temperature) and enthalpic elasticity $G\ell^3$ (G is the shear modulus of the material), thermally driven fluctuations become important enough to require a statistical treatment of their behavior in the context of physical polymers (2, 3), biopolymers such as DNA (4–6), etc. For filamentous objects that are relatively stiff, the worm-like chain (WLC) model (7–10), which assumes that polymer is a homogeneous elastic rod of circular cross-section with an energy density that scales quadratically in the local curvature, explains a range of experimental observations of the elasticity of DNA (4, 5, 11, 12) and similar biopolymers. Variations that have generalized the original WLC model also account for twisting and stretching deformations (13, 14), as well as the effects of fluctuations on filaments with spontaneous curvature and torsion (15), locally bistable behavior (16), etc., and go even further in explaining new observations of slender filaments in passive and active settings.

However, many biopolymers such as α helices, β sheets, graphene nanoribbons, and molybdenum ribbons (17–22) are physically ribbon-like, with their cross-sections better described by elongated rectangles rather than circles, and thus require a more sophisticated description beyond the WLC model that accounts for the anisotropic nature of the cross-section, such as the railway track model that couples two WLCs via transverse bonds (23–25). An alternative is to consider a continuum framework for ribbons, defined as slender structures whose thickness (h), width (w), and length (ℓ) are all widely separated, that is, $h \ll w \ll \ell$. In this setting, deformations of the ribbon will be almost isometric to the Euclidean plane; in the asymptotic limit of zero thickness, its mechanical energy density is solely a function of its mean curvature H, following symmetry considerations. At leading order, the energy of the ribbon can then be written as $(1/2)B\int(2H)^2 dA$, where $B = Eh^3/12(1-\nu^2)$ is the bending rigidity of the sheet (made of a material with Young's modulus E and Poisson ratio ν). If the ribbon is assumed to be developable, that is, it can be unrolled onto a flat state without stretching the midsurface anywhere, one can effectively integrate the energy in the width-wise direction and reduce it to a one-dimensional theory; this leads to an energy functional, first derived by Sadowsky (26), that is only a function of the curvature and torsion of the centerline (27).

The Sadowsky ribbon is isometric to a flat strip at all temperatures and encodes a nontrivial interaction between the local bend and twist degrees of freedom. At an

Author affiliations: [a]Division of Physics and Applied Physics, School of Physical and Mathematical Sciences, Nanyang Technological University, Singapore 637371; [b]Instituut-Lorentz, Universiteit Leiden, 2300 RA Leiden, The Netherlands; [c]School of Engineering and Applied Sciences, Harvard University, Cambridge, MA 02138; [d]Department of Physics, Harvard University, Cambridge, MA 02138; and [e]Department of Organismic and Evolutionary Biology, Harvard University, Cambridge, MA 02138

Author contributions: E.H.Y., L.G., and L.M. designed research; E.H.Y. and F.D. performed research; E.H.Y., F.D., and L.M. contributed new reagents/analytic tools; E.H.Y., F.D., L.G., and L.M. analyzed data; and E.H.Y., F.D., and L.M. wrote the paper.

The authors declare no competing interest.

This article is a PNAS Direct Submission. F.M. is a guest editor invited by the Editorial Board.

[1]To whom correspondence may be addressed. Email: eehou@ntu.edu.sg or lmahadev@g.harvard.edu.

This article contains supporting information online at https://www.pnas.org/lookup/suppl/doi:10.1073/pnas.2122907119/-/DCSupplemental.

Published August 2, 2022.

experiential level, the reader is invited to cut a long ribbon from a sheet of paper and convince herself of the asymmetry in the bend–twist coupling inherent in these objects: A ribbon can be bent without twisting, but cannot be twisted without bending. This is very different from the behavior of slender filaments with a circular cross-section, where the local twist is completely independent of the geometric torsion of the centerline (28), although there is a global relation between the two objects via a topological relation (29). While there has been increasing interest in the zero-temperature limit of the Sadowsky ribbon, starting about two decades ago (30–32), the role of finite temperature-driven fluctuations on the morphology of ribbons remains essentially unstudied, with one exception (33) that studied the statistical mechanics of a free ribbon. Here, we build on this observation to study the statistical mechanics of the Sadowsky ribbon under the effects of external forces and torques and understand the statistical morphology of fluctuating ribbons by characterizing its geometry and topology as a function of an appropriately scaled temperature and external loads.

Topology, Geometry, and Elasticity of a Ribbon

Topology. To understand the interplay between the geometry and topology of the ribbon, we recall the Călugăreanu–White–Fuller theorem Lk = Tw + Wr (29, 34, 35) which connects the number of times the two edges of the ribbon whirl around each other, described by the link (also known as linking number), Lk, a global quantity, to the sum of the integrated spatial rate of cross-section rotation, the total twist, Tw, and a global configurational integral that describes the nonplanarity of the configuration in terms of the writhe, Wr. For a fixed linking number, the conformations of the ribbon dictate how Lk is distributed between the degrees of freedom associated with Tw and Wr. We note that, for the WLC model, one would need to switch back to a "ribbon viewpoint" to estimate the linking number, but this ribbon is quite different from the double-helical ribbon-like structure of DNA.

Geometry. A slender ribbon, with $h \ll w \ll L$, can be parametrized in terms of the Frenet frame,

$$\mathbf{R}(s,\delta) = \mathbf{r}(s) + \delta\left[\mathbf{b}(s) + \frac{\tau(s)}{\kappa(s)}\mathbf{t}(s)\right], \qquad [1]$$

where $\mathbf{r}(s)$ represents the centerline of the ribbon, $s \in [0, L]$, L is the contour length, $\delta \in [-(w/2), w/2]$, $\kappa(s)$ is the curvature, $\tau(s)$ is its torsion, and $\mathbf{t}(s)$ and $\mathbf{b}(s)$ are the tangent and binormal vectors, respectively. The geometry of the ribbon can be characterized by its principal curvatures $\kappa_1(s,\delta)$ and $\kappa_2(s,\delta)$.

Elasticity. The assumption of developability, that is, that the ribbon can be unrolled and made flat without stretching anywhere, leads to the vanishing of the smaller principal curvature κ_2 everywhere, and the elastic energy of a thin ribbon reduces to the simple form $(1/2)B\int \kappa_1^2 dA$, which can be integrated effectively in the width-wise direction, resulting in the one-dimensional Sadowsky energy functional (26, 27, 31, 33, 36, 37),

$$E_{\text{Sadowsky}} = \frac{1}{2}Bw\int_0^L ds\,\frac{\left(\kappa^2(s)+\tau^2(s)\right)^2}{\kappa^2(s)}. \qquad [2]$$

We can then define the ribbon's configuration completely in terms of the curvature and torsion as a function of the arc length s along its centerline as shown in Fig. 1*B*, assuming that the flexural deformations are small enough to not worry about from self-intersections.

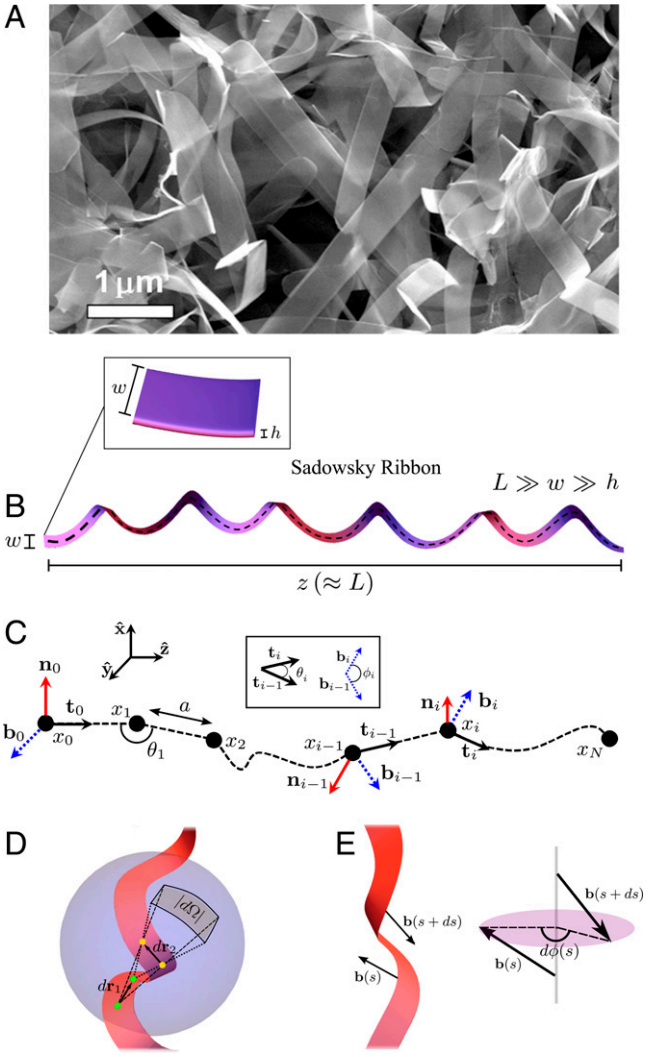

Fig. 1. (*A*) Graphene-coated ribbons of vanadium oxide. Image is courtesy of ref. 17. (*B*) The Sadowsky ribbon with relative extension z. Typical dimensions of the ribbon: $h \approx 1$nm, $w \approx 10$ nm, and $L \approx 10\mu$m; hence $L \gg w \gg h$. The smooth ribbon is generated using *BSplineFunction* in Mathematica. (*Inset*) The width w is much larger than the thickness h. (*C*) A discrete ribbon model consist of $N+1$ vertices, $\mathbf{x}_0, \mathbf{x}_1, \ldots \mathbf{x}_N$, and an orthogonal Frenet frame $\mathbf{F}_i = (\mathbf{t}_i, \mathbf{n}_i, \mathbf{b}_i)$ at each vertex. The distance between adjacent vertices is $|\mathbf{x}_{i+1} - \mathbf{x}_i| = a$. Typically $w/a \approx 1$. (*Inset*) The angle between $\mathbf{t}_{i-1}$ and $\mathbf{t}_i$ is θ_i; the angle between $\mathbf{b}_{i-1}$ and $\mathbf{b}_i$ is ϕ_i. (*D*) Writhe, Wr, is the Gauss double integral of the solid angle $d\Omega$ determined by the crossing of $d\mathbf{r}_1$ and $d\mathbf{r}_2$ about each other. (*E*) Twist, Tw, is the integral of the angle of rotation $d\phi$ of the vector $\mathbf{b}(s)$ about the centerline of the ribbon.

We choose a reference state with zero curvature and torsion not only for simplicity but also because this functional reduces to that for the planar *Elastica*, when $\tau = 0$. We note that this energy functional is quite different from that for a three-dimensional elastic filament which has an additional term quadratic in the twisting strain (which is not the geometric torsion of the centerline in general). Furthermore, in this limit, the ribbon is achiral (i.e., invariant under mirror reflection) in the absence of any external applied torque. However, for isometric deformations of a ribbon, the geometric torsion is exactly equal to the local twist, since the Frenet frame associated with the centerline coincides with the material frame attached to the cross-section (30). The torsional and flexural deformations are nonlinearly (and asymmetrically) coupled such that the ribbon can store curvature when untwisted (i.e., $\kappa \neq 0$, $\tau = 0$), but it becomes energetically prohibitive to store torsion in the presence of a vanishing curvature (i.e., $\kappa \approx 0$, $\tau \neq 0$).

Boundary Loading. In the presence of applied end forces and torques, we assume that one end of the ribbon is anchored (fixed boundary) and the other end experiences an applied force $\mathbf{F} = F\hat{\mathbf{z}}$ ($F > 0$) and a torque Ω, resulting in two additional terms to the free energy,

$$E_{\text{force}} = -\mathbf{F} \cdot \int_0^L \mathbf{t}(s)\, ds = -Fz, \quad [3]$$

$$E_{\text{torque}} = -2\pi\Omega \text{Lk}, \quad [4]$$

where z is the end-to-end extension of the ribbon along $\hat{\mathbf{z}}$ (8, 9), and Lk is the link of the open ribbon (38). The applied torque acts as a chemical potential for Lk and couples the bend and twist fluctuations, similar to earlier approaches (13, 14) where the desired link is achieved by tuning the applied torque on the ribbon. Then the complete energy functional for the ribbon is given by

$$E_{\text{ribbon}} = E_{\text{Sadowsky}} + E_{\text{force}} + E_{\text{torque}}. \quad [5]$$

Here we have ignored excluded volume interactions which can become particularly important when the ribbon is either long relative to the persistence length, weakly stretched, and/or entangled.

Computational Model of a Ribbon

Discrete Model. In order to understand the implications of the theory for the conformational phase space of the ribbons, we discretize the ribbon along its centerline into a chain of N segments with $N+1$ vertices $\{\mathbf{x}_0, \mathbf{x}_1, \ldots, \mathbf{x}_N\}$ separated by a fixed length a as shown in Fig. 1*C*, where a is the length of each segment and $L = Na$. For each pair of nearest-neighbor vertices $\mathbf{x}_{i-1}$ and $\mathbf{x}_i$, we define the unit tangent vector as $\mathbf{t}_i = (\mathbf{x}_i - \mathbf{x}_{i-1})/|\mathbf{x}_i - \mathbf{x}_{i-1}|$, for $i = 1, \ldots, N$. Next, we define the discrete bending angle θ_i by $\cos\theta_i = \mathbf{t}_i \cdot \mathbf{t}_{i-1}$ and the discrete bond angle ϕ_i by $\cos\phi_i = \mathbf{b}_i \cdot \mathbf{b}_{i-1}$. At each vertex, there is an orthonormal discrete Frenet frame $\boldsymbol{F}_i = (\mathbf{t}_i, \mathbf{n}_i, \mathbf{b}_i)$ as shown in Fig. 1*C*. The Frenet frames $\boldsymbol{F}_i$ are orthogonal 3×3 matrices, whose column vectors are $\mathbf{t}_i, \mathbf{n}_i$ and $\mathbf{b}_i$. We can write down an iterative relation between two adjacent discrete Frenet frame (33, 39): $\boldsymbol{F}_i = \boldsymbol{F}_{i-1}\boldsymbol{R}_i$, where

$$\boldsymbol{R}_i = \begin{pmatrix} \cos\theta_i & -\sin\theta_i & 0 \\ \sin\theta_i\cos\phi_i & \cos\theta_i\cos\phi_i & -\sin\phi_i \\ \sin\theta_i\sin\phi_i & \cos\theta_i\sin\phi_i & \cos\phi_i \end{pmatrix}. \quad [6]$$

The discrete curvature at vertex i can be calculated using $\kappa_i^2 = a^{-2}|\mathbf{t}_i - \mathbf{t}_{i-1}|^2 = 2a^{-2}(1 - \cos\theta_i)$. Similarly, the discrete torsion is given by $\tau_i^2 = a^{-2}|\mathbf{b}_i - \mathbf{b}_{i-1}|^2 = 2a^{-2}(1 - \cos\phi_i)$. The discretized version of the elastic energy functional described by Eqs. **2–5** is

$$\frac{E_{\text{ribbon}}}{k_B T} = \frac{Bw}{ak_B T}\sum_{i=1}^{N-1}\frac{[(1-\cos\theta_i) + (1-\cos\phi_i)]^2}{(1-\cos\theta_i)} - \frac{Fa}{k_B T}\sum_{i=0}^{N-1}\mathrm{t}_i^z - \frac{2\pi\Omega}{k_B T}\text{Lk}, \quad [7]$$

where t_i^z is the z component of the ith tangent vector, k_B is the Boltzmann constant, and T is the temperature (*SI Appendix*, section S1).

To track the geometry and topology of the ribbon, we also define discrete analogs of the Tw via a cumulative twist density function as (40)

$$T(n) = \frac{1}{2\pi}\sum_{i=1}^{n-1}(\mathbf{b}_{i-1} \times \mathbf{b}_i) \cdot \mathbf{t}_i, \quad [8]$$

where the positive direction of rotation is defined by the right-hand rule; that is, $\text{sign}[(\mathbf{b}_{i-1} \times \mathbf{b}_i) \cdot \mathbf{t}_{i-1}]$. The cumulative twist density function specifies how each segment of the ribbon contributes to the overall twist as we move from one end of the ribbon to the other end. When $n = N$, the cumulative twist density function is identical to the twist; that is, $T(N) = \text{Tw}$. Similarly, we define the cumulative writhe density function as

$$W(n) = \frac{1}{2\pi}\sum_{i=2}^{n-1}\sum_{j<i}\Omega_{ij}, \quad [9]$$

where Ω_{ij} is the Gauss integral along the segments $a\mathbf{t}_i$ and $a\mathbf{t}_j$, and is calculated according to the protocol in ref. 40. When $n = N$, the cumulative writhe density function is identical to the writhe; that is, $W(N) = \text{Wr}$. Finally, the cumulative link density function is

$$L(n) = T(n) + W(n), \quad [10]$$

and $L(N) = \text{Lk}$. The cumulative density functions thus inform us how each segment of the ribbon contributes to the overall link, twist, and writhe.

Parameter Values. Under the assumption that biopolymers can be viewed as a continuum of elastic objects on scales large relative to their molecular constituents, we use the following parameter values for ribbons: Young's modulus E $\approx$ 100 MPa to 1,000 MPa, $h \approx 1$ nm, and $F \sim 0.01\ k_BT$/nm to $10\ k_BT$/nm (4, 8, 41, 42). For our ribbon-like polymer model, $a \approx 10$ nm, $w/a \approx 1$, and $Bw/k_BT \approx 10$ nm. It is useful to define new dimensionless parameters, Λ (normalized temperature), f (normalized force), and Γ (normalized torque) as follows:

$$\Lambda = \frac{ak_BT}{Bw}, \quad f = \frac{Fa^2}{Bw}, \quad \Gamma = \frac{\Omega a}{Bw}. \quad [11]$$

They can be mapped to the original parameters via $f/\Lambda = Fa/k_BT$ and $\Gamma/\Lambda = \Omega/k_BT$. For this work, we will use these dimensionless parameters exclusively. In our study, we set temperature $\Lambda \in [0.1, 1.5]$, force $f \in [0, 10]$, $\Gamma \in [-8, 8]$, and $N = 100$. We find that this particular choice of N is sufficient to capture relevant physics that govern our discretized polymer chain (*SI Appendix*, Figs. S1, S9, and S13).

Monte Carlo Simulations. The ribbon is initialized with random orientations, with one end of the chain fixed, namely, $\boldsymbol{F}_0 = (\mathbf{t}_0, \mathbf{n}_0, \mathbf{b}_0) = (\hat{\mathbf{z}}, \hat{\mathbf{x}}, \hat{\mathbf{y}})$, and the other chains free to take on arbitrary conformations. During the first step, we randomly picked two new angles θ_1 and ϕ_1, and update the adjacent Frenet frame $\boldsymbol{F}_1 = \boldsymbol{F}_0\boldsymbol{R}_1$ as well as the position of the next vertex, $\mathbf{x}_2$. This configuration is accepted via a Metropolis algorithm (43). We then proceed to the next link and repeat the process. This procedure terminates when we reach the end of the chain, and this constitutes one Monte Carlo sweep. For our simulations, we performed 10^6 Monte Carlo sweeps per chain, the first half of which is devoted to equilibration. In our simulations, we have ignored the effects of knotting, since the discrete chain segments are allowed to cross one another during trial moves in the Monte Carlo simulation. We can close the open ribbon using the minimally interfering closure scheme (44). One would need to evaluate the Alexander polynomial for knot checking and reject any trial moves that change the topology of the chain. Such a test is omitted in this study, as it has been found that such an effect is not too significant, and topology checking is computationally intensive (11, 13, 45).

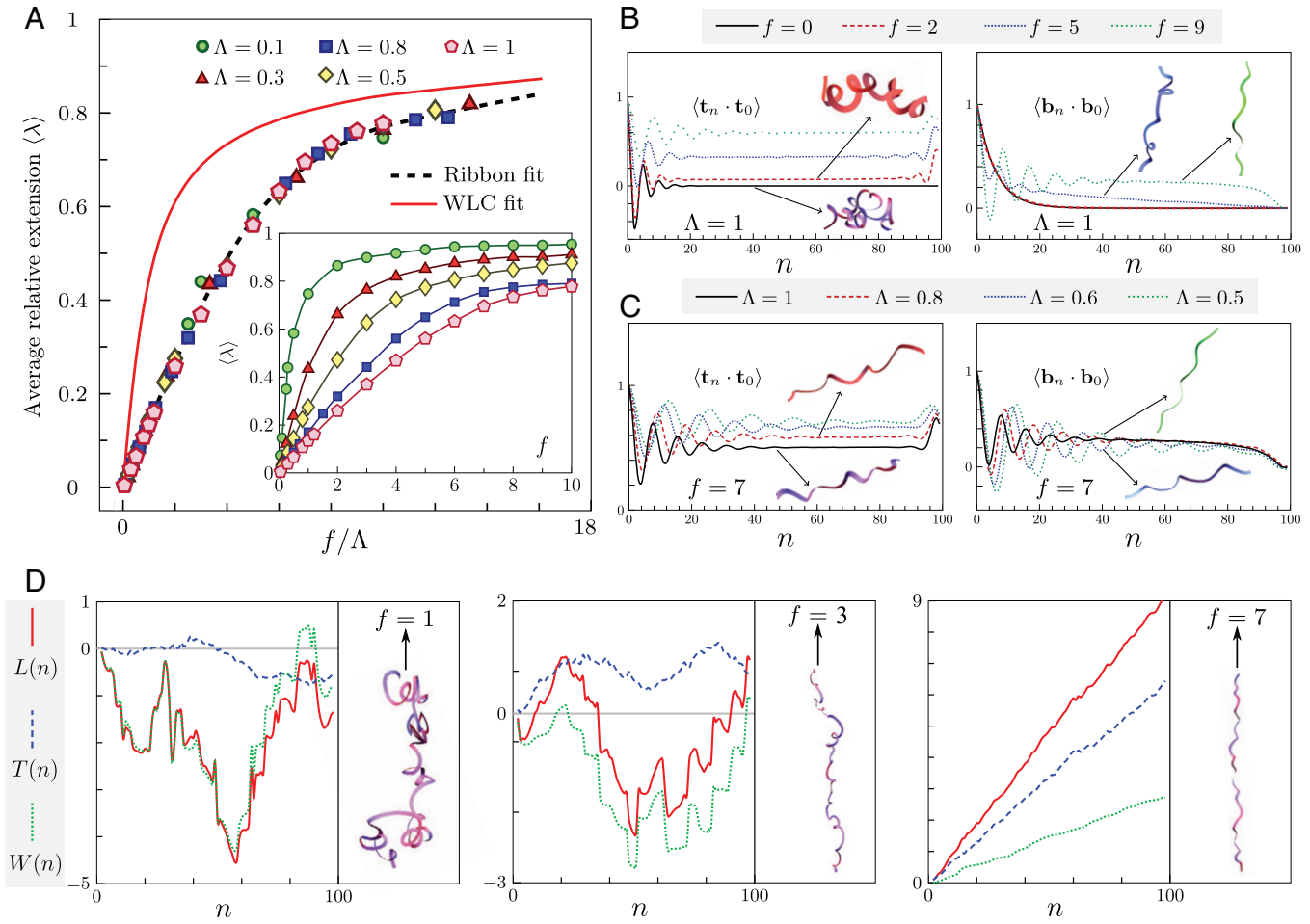

Fig. 2. (*A*) The average relative extension $\langle\lambda\rangle$ as a function of different forces f and temperatures Λ collapses onto a single curve (dashed line) fitted by Eq. **14**. (*Inset*) The force-extension curves for different temperatures, λ. (*B*) Tangent–tangent $\langle \mathbf{t}_n \cdot \mathbf{t}_0\rangle$ and binormal-binormal $\langle \mathbf{b}_n \cdot \mathbf{b}_0\rangle$ correlation functions from Monte Carlo simulations of a ribbon-like polymer chain of $N = 100$ segments at fixed temperature $\Lambda = 1$ and different applied forces. (*C*) The $\langle \mathbf{t}_n \cdot \mathbf{t}_0\rangle$ and $\langle \mathbf{b}_n \cdot \mathbf{b}_0\rangle$ for $f = 7$ ($f > f_c$) are plotted at different temperatures. (*D*) The cumulative density functions, $L(n)$, $T(n)$, and $W(n)$, along the ribbon for (*Left*) $f = 1$ (HW phase), (*Middle*) $f = 3$ (HW phase), and (*Right*) $f = 7$ (HT phase) at $\Lambda = 1$. The ribbon conformation is depicted beside each set of curves. The ribbon undergoes phase transition from HW to HT as we increase the force f. The critical force $f_c \approx 5$.

Ribbon under Tension

Force–Extension Relations. We first consider a ribbon-like polymer that is subject to an applied force without any external torque. A microscopic polymer chain behaves very differently from its macroscopic counterpart in that it is under constant thermal fluctuations, which prevents the chain from being straight. Every Fourier mode of its shape is excited according to the equipartition theorem. Because the ribbon is never straight, its average shape will respond as soon as any stress is applied. There is no threshold, and it can bend and twist freely to relieve stresses.

In the limit of low force ($f/\Lambda < 1$), the ribbon is in a random coil configuration and behaves like a linear spring with an elasticity that arises from entropy. Fitting our simulations to the low force regime shows that the effective spring constant connecting the applied force F to the relative extension $\lambda = z/L$ is given by $k \approx 7.15 k_B T/a$ as shown in Fig. 2*A*. In terms of dimensionless parameters, this expression reads as

$$\frac{f}{\Lambda} = \frac{Fa}{k_B T} \approx 7.15\frac{z}{L} = 7.15\lambda. \qquad [12]$$

Evidently, the Sadowsky ribbon is stiffer than the WLC, which obeys $f/\Lambda = (3/2)\lambda$ in the limit of small force, thus requiring a much greater force to realize a given extension. The ribbon becomes harder to stretch as the temperature Λ increase. As we increase the force, the force–extension curves become nonlinear. At higher forces ($f/\lambda > 10$), the relative extension begins to level off as it approaches unity. At this point, the ribbon has been stretched nearly straight. The relative extension λ asymptotes toward one with a distinctive $1/\sqrt{F}$ behavior. In these regards, the Sadowsky ribbon is qualitatively similar to the WLC. The force–extension curves at different temperatures collapse into one universal curve, as shown in Fig. 2*A* (*SI Appendix*, section S2). The best-fit interpolation formulas for the WLC (8) and Sadowsky ribbon as a function of z/L are given by

$$\frac{Fa}{k_B T} = \frac{1}{4(1-\lambda)^2} + \lambda - \frac{1}{4} \quad \text{(WLC)}, \qquad [13]$$

$$\frac{Fa}{k_B T} = \frac{0.27}{(1-\lambda)^2} + 6.60\lambda - 0.27 \quad \text{(Ribbon)}. \qquad [14]$$

Geometrical Correlations. The tangent–tangent correlation function, $\langle \mathbf{t}_n \cdot \mathbf{t}_m\rangle$, measures the correlations between the unit tangent at vertex n and the unit tangent at vertex m; values close to one indicate high correlations, while zero indicates no correlation. Since all the tangent vectors are equivalent, we compute $\langle \mathbf{t}_n \cdot \mathbf{t}_0\rangle$ for convenience. If the correlation length, ℓ, which is the distance over which fluctuations in one region of space are correlated

or affected by those in another region, is over multiple chain segments, the ribbon is said to exhibit long-range order; otherwise, the ribbon is said to be disordered. A previous study (33) has shown that the tangent–tangent correlation function, $\langle \mathbf{t}_n \cdot \mathbf{t}_0 \rangle$, is oscillatory when $f = \Gamma = 0$; in fact, this is true for any finite f and Λ, as shown in Fig. 2 *B* and *C*. This means that the polymer model has an underlying long-range ordered helical structure as long as there is no applied torque. For segments sufficiently far from the end segment, $\langle \mathbf{t}_n \cdot \mathbf{t}_0 \rangle$ can be effectively described by

$$\langle \mathbf{t}_n \cdot \mathbf{t}_0 \rangle = e^{-s/\ell_p} \cos(ks) + M, \qquad [15]$$

where $s = na$, k is the wavenumber, ℓ_p is the persistence length characterizing the length scale over which orientational correlations persist, and M is a parameter that indicates residual tangential long-ranged order. In the absence of external forces, the persistence length $\ell_p \approx a\Lambda^{-1}$ and the wavenumber $k \approx a^{-1}\Lambda^{1/2}$ (33). In addition, the orientational correlation along the ribbon decays to zero; that is, $\langle \mathbf{t}_n \cdot \mathbf{t}_0 \rangle \to 0$ for $n \to \infty$, implying a lack of long-ranged order ($M = 0$). In contrast, at finite forces $f \neq 0$, the tangent–tangent correlation function approaches a finite value; that is, $\langle \mathbf{t}_n \cdot \mathbf{t}_0 \rangle \to M \neq 0$ for $n \to \infty$, indicating long-range orientational order. The asymptotic value M, in turn, decreases as we increase the temperature, indicating a loss of long-range order, as shown in Fig. 2*C*. The tangent vector of the end segment $\mathbf{t}_N$ and its neighboring segments tend to align with the applied force $\boldsymbol{F} = F\hat{\mathbf{z}}$. Since $\mathbf{t}_0 = \hat{\mathbf{z}}$, this explains the peaks in tangent–tangent correlation function near the end segment. On the other hand, the wavenumber k at fixed Λ gets smaller for a higher f, and eventually becomes smaller than the unit separation between the segments (*SI Appendix*, section S4).

While $\langle \mathbf{t}_n \cdot \mathbf{t}_0 \rangle$ is always oscillatory, we observe striking differences in behavior for the binormal–binormal correlation function $\langle \mathbf{b}_n \cdot \mathbf{b}_0 \rangle$. When $f = \Gamma = 0$, $\langle \mathbf{b}_n \cdot \mathbf{b}_0 \rangle$ exhibits exponential decay at any nonzero temperature Λ; however, this is no longer true when f is nonzero, as plotted in Fig. 2 *B* and *C*. As we increase f at fixed Λ, we observe that $\langle \mathbf{b}_n \cdot \mathbf{b}_0 \rangle$ experiences a transition at some critical force $f_c = f_c(\Lambda)$, going from (pure) exponential decay to oscillatory decay. The binormal–binormal correlation function can be described as

$$\langle \mathbf{b}_n \cdot \mathbf{b}_0 \rangle = \begin{cases} e^{-s/\ell_\tau}, & f < f_c(\Lambda) \\ e^{-s/\ell_\tau} \cos(k_\tau s) + M_\tau, & f > f_c(\Lambda) \end{cases}, \qquad [16]$$

where ℓ_τ, k_τ, and M_τ are the torsional persistence length, torsional wavenumber, and torsional LRO parameter, respectively (*SI Appendix*, sections S2 and S5).

Ribbon Morphologies and Chirality. Even though the Sadowsky ribbon is achiral, individual torsional fluctuations will not be inversion symmetric, and different segments of the ribbon will exhibit different handedness. Two adjacent helical structures with opposite handedness are connected by a perversion, a chirality-reversing localized defect, which is a classical motif commonly observed in such instances as tangled telephone cords and plant tendrils (46–48). The ribbon will have segments of alternating chirality connected by perversions; along portions of the ribbon with right-handed (left-handed) helicity, $W(n)$ will increase (decrease) monotonically. Without perversions, the cumulative writhe density function can only change monotonically; at each perversion, the change in the cumulative writhe density function changes sign. Under a small applied force ($f = 1$; Fig. 2*D*, *Left*), the ribbon is extremely coiled up, yet the twist and writhe are small, around $O(1)$ in magnitude. The fluctuations in the cumulative twist density function are significantly smaller than that in the cumulative writhe density function. Through the proliferation of perversions, a ribbon that is bent and twisted at low applied force can achieve a small link. Because the link is not constrained by an external torque, it can be expelled from the free boundary (38). We identify these kinds of conformations as the writhe-dominated helical phase (HW), noting that it is the large change in cumulative writhe density function and the large numbers of perversions that capture the character of the ribbon conformations. In the HW morphological phase at zero applied torque, the link, twist, and writhe are typically close to zero (*SI Appendix*, section S11).

As we increase the applied force, the ribbon becomes increasingly stretched, with a smaller number of perversions, and the fluctuations in the cumulative twist density function become more significant. At the critical force ($f = 5$; Fig. 2 *D*, *Middle*), the variations in cumulative twist density function become comparable to the cumulative writhe density function, and we categorize the ribbon as simply in the helical state. Under forces greater than f_c ($f = 7$; Fig. 2 *D*, *Right*), the ribbon is nearly straight and has very few perversions. Simultaneously, the fluctuations in the cumulative link, twist, and writhe functions are increasingly suppressed and increase (decrease) monotonically if the helicity of the ribbon is right handed (left handed). At zero torque, the ribbon can have either handedness, as a result of the symmetry of the ribbon under parity. Here, we have used a right-handed conformation for illustration; in fact, the mirror image of this conformation is equally likely. In this case, we observe that Tw ≈ 6, Wr ≈ 3, and Lk ≈ 9. This phenomenon is similar to the observation that the writhe in a helical telephone cord is converted into twist when stretched. We term such morphologies the helical phase that is twist-dominated (HT). Thus, the Sadowsky ribbon at zero torque may exist either in the long-range ordered HT where Tw $>$ Wr $\approx O(1)$ or HW where Wr $\approx$ Tw ≈ 0, depending on f and Λ. Generally, we observe that high/low force leads to HT/HW, and the transition point $f_c(\Lambda)$ occurs when the binormal–binormal correlation function changes from (pure) exponential decay to oscillatory decay. The cumulative density functions allow us to investigate the formation of perversions as we move along the arc length of the ribbon. In our model, the morphological cross-over is also accompanied by a spontaneous breaking of the symmetry of the ribbon under parity, which will be discussed later in the next section.

Ribbon under Tension and Torque

Force–Extension Relations under Torque. A macroscopic elastic rod under torque and tension remains straight as long as the twisting couple is below a critical value $\Omega_{\text{critical}} \propto \sqrt{F}$ (13, 14, 28). On the other hand, a microscopic ribbon under tension and torque behaves very differently, as there is no threshold to bending or twisting. In this case, the twisting couple term breaks the parity symmetry of the Sadowsky functional: $\Omega > 0$ will lead to a right-handed ribbon, while $\Omega < 0$ will result in a left-handed ribbon. The twisting couple will push fluctuations with the same handedness closer to instability, while suppressing those of the opposite handedness, and ribbon conformations with the same helicity as the applied torque will be favored. These twist fluctuations will, in turn, affect the bend fluctuations, due to the coupling between the curvature and torsional modes of the Sadowsky ribbon. The end result will be a coupling between the applied torque and the mean end-to-end extension of the polymer.

The force–extension curve of our polymer chain is shown in Fig. 3*A* together with characteristic conformations of the ribbon for $\Lambda = 1$, and different Γ. Under small applied torques, the

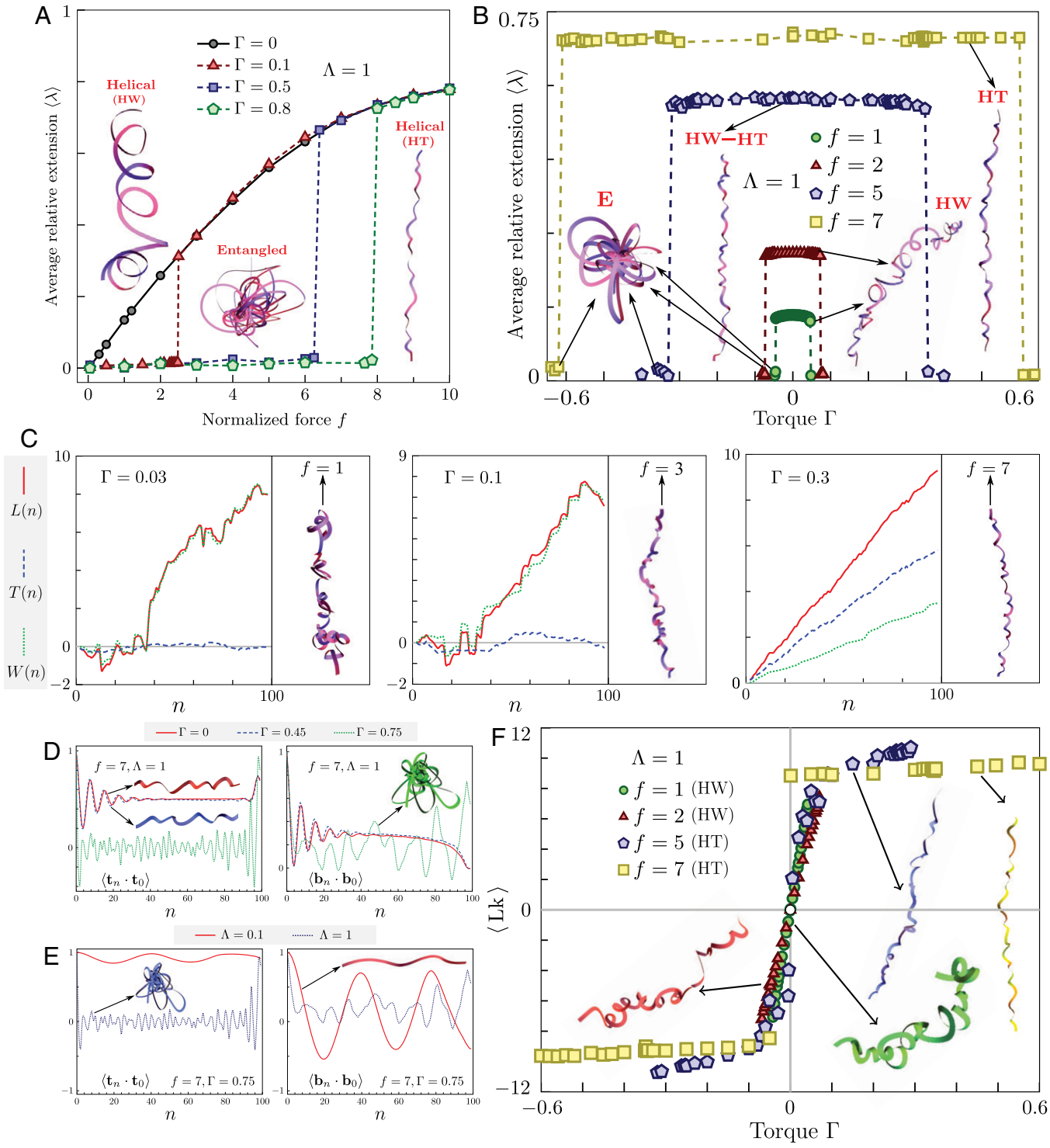

Fig. 3. (*A*) The force-extension curves for a ribbon at temperature $\Lambda = 1$ and different applied torques Γ. (*B*) Average relative extension $\langle\lambda\rangle$ vs applied torque Γ of a ribbon at fixed temperature $\Lambda = 1$ for different applied forces f. The helical phase is stable for $\Gamma \in [-\Gamma_c(f,\Lambda), \Gamma_c(f,\Lambda)]$; otherwise the ribbon is entangled. (*C*) The cumulative density functions, $L(n)$, $T(n)$, and $W(n)$, along the ribbon for (*Left*) $f = 1$ and $\Gamma = 0.03$ (HW phase), (*Middle*) $f = 3$ and $\Gamma = 0.1$ (HW phase), and (*Right*) $f = 7$ and $\Gamma = 0.3$ (HT phase) at $\Lambda = 1$ for different torques Γ. (*D*) Tangent–tangent and binormal–binormal correlation functions corresponding to $f = 7$ and $\Lambda = 1$ for different torque Γ. The phase transition occurs at $\Gamma_c \approx 0.62$. (*E*) The $\langle \mathbf{t}_n \cdot \mathbf{t}_0 \rangle$ and $\langle \mathbf{b}_n \cdot \mathbf{b}_0 \rangle$ for $f = 7$ ($f > f_c$) and $\Gamma = 0.75$ are plotted at different temperatures. (*F*) Plot of average link vs. torque at $\Lambda = 1$. For $f < f_c$, the average link varies continuously with applied torque. At critical force $f_c = 5$, the slope approaches infinity. For $f > f_c$, the average link is discontinuous, and the jump in $\langle \mathrm{Lk} \rangle$ at zero applied torque is indicative of a first-order phase transition. At zero torque, parity symmetry is spontaneously broken at large f, and the ribbon adopts a particular handedness. At low forces ($f = 1, 2$), the ribbon is predominantly in the HW phase, while, at large forces ($f = 5, 7$), the ribbon is predominantly in the HT phase. In contrast with the case shown here, for $\Lambda = 1$, the case $\Lambda \gg 1$ leads to a mostly entangled phase at finite torque, while the case $\Lambda \ll 1$ leads to an ordered helical phase (typically HT) at finite torque (Fig. 4).

ribbon is in the HT phase at high force. As we reduce the force, there is a cross-over from twist to writhe, and the ribbon typically becomes shorter and more coiled and transits from HT phase to HW phase. Under zero torque, the ribbon will shift from HT to HW phase under decreasing applied force; for nonzero torque, the ribbon rapidly goes into an entangled phase (E) below a minimum force $f_c(\Gamma, \Lambda)$. This transition into entangled phase may occur from either the HT or HW phase, depending on

the force, torque, and temperature. The entangled morphological phase is characterized by its small relative extension ($\lambda \ll 1$). As we do not include steric effects, the ribbon in the entangled phase collapses into a small globule. Due to self-crossing, the topology of the ribbon will be heavily knotted. The helix to entangled transition is abrupt, reminiscent of a first-order phase transition, and critical force becomes smaller with either decreasing torque or decreasing temperature (*SI Appendix*, sections S6 and S7).

The average relative extension of the ribbon $\langle\lambda\rangle$ under varying torque Γ for different values of f and Λ is shown in Fig. 3*B*. Due to the assumption of developability, the relative extension is an even function of the applied torque. A ribbon under high applied force (yellow squares, Fig. 3*B*) is stable in the HT phase as long as $\Gamma < |\Gamma_c(f,\Lambda)|$; otherwise, it becomes entangled. In the HT phase, increasing the torque does not result in significant changes to the ribbon conformations. The change in relative extension while in the helical phase is relatively small, $\Delta\lambda = \lambda_{\max} - \lambda_{\min} \approx 0.02$. As we reduce the applied force, the helical phase remains stable for a smaller range of applied torque; that is, $\Gamma_c(f,\Lambda)$ reduces with decreasing applied force (*SI Appendix*, section S6).

Statistical Topology of Ribbons. Under a small applied force and torque ($f = 1$, $\Gamma = 0.03$; Fig. 3 *C*, *Left*), the ribbon is coiled in a random manner. We observe that the cumulative writhe density function is significantly larger than the cumulative twist density function, and the ribbon is evidently in the HW phase. Due to the symmetry-breaking torsional constraint term, right-handed fluctuations will be favored: Ribbon segments with right-handed chirality tend to be extended over many discrete segments while those with left-handed chirality are generally short ranged. The overall chirality of the ribbon is right handed, resulting in a nonzero, positive link in this case. The twist of the ribbon is close to zero, and the writhe provides the leading contribution to the link of the ribbon. A similar behavior is observed at $f = 3$ and $\Gamma = 0.1$ (HW phase), as observed in Fig. 3 *C*, *Middle*. Unlike the zero-torque case considered in the previous section, the HW phase under torque has a finite writhe; that is, $\mathrm{Wr} \approx O(1)$ and $\mathrm{Tw} \approx 0$. As we increase the applied force and torque ($f = 7$, $\Gamma = 0.3$), the ribbon becomes elongated and transitions into the HT phase, as seen in Fig. 3 *C*, *Right*, and $\mathrm{Tw} > \mathrm{Wr} \approx O(1)$. We observe the disappearance of perversions, and the cumulative density functions are generally monotonic. The ribbon has a right-handed helicity, with the twist as the predominant contributor to the link in this case (*SI Appendix*, sections S11 and S12).

Geometrical Correlations. In the helical phase (HW/HT), the correlation functions $\langle \mathbf{t}_n \cdot \mathbf{t}_0 \rangle$ and $\langle \mathbf{b}_n \cdot \mathbf{b}_0 \rangle$ obey Eqs. **15** and **16**, respectively. In the entangled phase, $\langle \mathbf{t}_n \cdot \mathbf{t}_0 \rangle$ and $\langle \mathbf{b}_n \cdot \mathbf{b}_0 \rangle$ exhibit disordered behaviors, as shown in Fig. 3*D*. The transition occurs at a torque $\Gamma_c(f,\Lambda)$ that defines the "Lifshitz point" (24, 33) that divides the disordered entangled phase and the ordered helical phase. The transition may be achieved either by varying the force at fixed temperature and torque $f_c(\Gamma,\Lambda)$, changing the torque at fixed temperature and force $\Gamma_c(f,\Lambda)$ (Fig. 3*D*), or changing the temperature at fixed force and torque $\Lambda_c(f,\Gamma)$ (Fig. 3*E*).

In the presence of force, we observe that both ℓ_p and ℓ_τ are approximately constant in the HW phase and scale as $f^{-1/2}$ in the HT phase. Interestingly, the high f limit is similar to that of the Moroz–Nelson model (13). We find that k scales as $(f^2 + C)^{-1}$ over all f, where C is a temperature-dependent constant that keeps k finite in the low-force limit; k_τ vanishes in HW phase and scales as f^{-2} in the HT phase. The temperature dependence at finite f appears to be identical to the $f = 0$ case: Both ℓ_p and

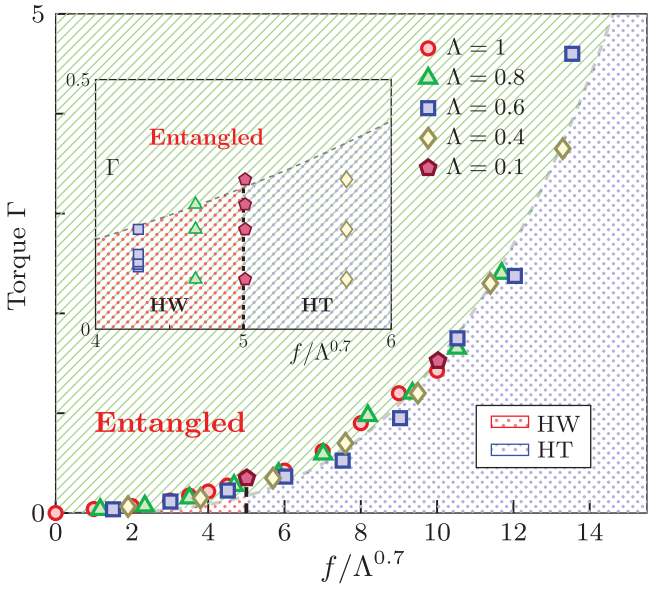

Fig. 4. Morphological phase diagram of the ribbonlike polymer subject to different torques Γ, forces f, and temperatures Λ. Three morphological phases exist: writhe-dominated helical (HW), twist-dominated helical (HT), and entangled (E). The transition between HW and HT is continuous with a phase boundary at $f \approx 5\Lambda^{0.7}$. The transition between HW/HT and E is abrupt and the phase boundary collapses onto a universal curve $\Gamma_c(f,\Lambda) = g(f/\Lambda^{0.7})$ where $g(x) \sim x^3$.

ℓ_τ scale as Λ^{-1}, k scales as $a\Lambda^{1/2}$ in either helical phase, and k_τ scales as $a^{-1}\Lambda^{1/2}$ in HT phase. Finally, we observe that ℓ_p, ℓ_τ, k, and k_τ do not seem to vary appreciably with Γ in the range investigated in this work. More details can be found in *SI Appendix*, sections S4 and S5.

Phase Transition with Lk as the Order Parameter. The variation of $\langle \mathrm{Lk} \rangle$ of the ribbon in the helical phase at fixed temperature with the applied torque Γ is shown in Fig. 3*F*. At forces below the critical force f_c, the ribbon has a zero average link at zero torque. The link exhibits a linear dependence on the applied torque. At forces above f_c, there is a jump in $\langle \mathrm{Lk} \rangle$ at zero applied torque, indicative of a first-order phase transition; that is, $\langle \mathrm{Lk} \rangle = \pm \mathrm{Lk}_0$ at $\Gamma = 0$. The link changes slightly with the applied torque and asymptotes to a constant that represents the maximum link admissible to the chain with N finite segments in helical phase (*SI Appendix*, Fig. S9). At f_c, $\langle \mathrm{Lk} \rangle$ is continuous at $\Gamma = 0$ but has an infinite slope. This is analogous to what happens in ferromagnets: The magnetization varies discontinuously with the applied field when the temperature is below the Curie temperature T_C (ferromagnetic phase), while the magnetization varies smoothly when $T > T_\mathrm{C}$ (paramagnetic phase). Thus, we can interpret the average link $\langle \mathrm{Lk} \rangle$ as the order parameter of the ribbon-like polymer and interpret the torque Γ as the conjugate field. In the HW morphological phase at zero torque, the ground state of the ribbon has zero link; that is, $\langle \mathrm{Lk} \rangle = 0$, and the system exhibits chirality. However, in the HT phase at zero torque, the ground state becomes doubly degenerate, and the ribbon commits to one of the two minima ($\pm \mathrm{Lk}_0$) randomly, resulting in the spontaneous breaking of chirality. Unlike in the simple ferromagnet where the transition is controlled by the strength of external field, the morphological transition of the ribbon-like polymer can be achieved by either tuning temperature, force, or torque.

Morphological Phase Diagram. Our study shows that the Sadowsky ribbon exhibits a rich morphological phase diagram

that spans the torque–force–temperature phase space as shown in Fig. 4. There are three phases in the ribbon-like polymer: HW at low force and low torque, HT at high force and low torque, and the entangled phase at high torque. Both helical phases are ordered, while the entangled phase is disordered. At zero torque, the ribbon conforms to either HW or HT phase at all finite f and Λ. In the HW phase at zero torque, the ground state of the ribbon is chiral with zero average link with multiple perversions, while, in the HT phase, the ribbon relaxes into either one of two minima ($\pm$ Lk$_0$), and parity symmetry is spontaneously broken. The transition occurs at $f_c(\Lambda)$ whereby the binormal–binormal correlation function changes from (pure) exponential decay to oscillatory decay.

At finite torque, the HW phase is characterized by its small relative extension, small average link, tangent–tangent correlation function that is oscillatory, and binormal–binormal correlation function that is purely exponential decay. The link is shown to increase with the applied stresses, and the ribbon has finite writhe and small twist. There are multiple perversions that flip the chirality of the ribbon, and its overall handedness conforms to that of the applied torque, since fluctuations with the same handedness are favored. In the HT phase, the ribbon-like polymer has a large relative extension ($\langle\lambda\rangle \to 1^-$), finite $\langle$Lk$\rangle$ (Tw $>$ Wr), and oscillating correlation functions. The ribbon tends to be straight as a consequence of the nonlinear coupling term τ^4/κ^2 which forces τ to approach zero faster than κ. The ribbon has few, if any, perversions, and the link changes marginally from $\pm$ Lk$_0$ under applied stresses. The ribbon-like polymer in HW/HT phase experiences very small variations in its relative extension under variation in torque. The transition between HW and HT phase is continuous, and the phase boundary occurs at $f \approx 5\Lambda^{0.7}$, independent of the applied torque. It is stable until a critical torque $\Gamma_c(f,\Lambda)$, beyond which the ribbon starts to get entangled, reminiscent of a first-order phase transition. In the entangled phase, the polymer has extremely small $\langle\lambda\rangle$, diverging $\langle$Lk$\rangle$, and correlation functions with random oscillations. The transition between HW/HT and E phase is abrupt, and the phase boundary collapses onto a universal curve $\Gamma_c(f,\Lambda) = g(f/\Lambda^{0.7})$ for $0 \le f/\Lambda^{0.7} \le 16$, where $g(x) \approx x^3$ is a function of one variable. The data were fitted to Ax^B, with $A = 0.0011 \pm 0.0002$, $B = 3.14 \pm 0.08$, and adjusted R-squared ≈ 0.98 (*SI Appendix*, section S10).

Conclusions

Ribbon-like polymers whose thickness, width, and length are all well separated are mechanically well characterized by the Sadowsky functional, and are known to have unusual static responses due to the constraints of effectively inextensional deformations. Here, we build on this and describe the statistical geometry and topology of thermal ribbons subjected to an applied load and torque, and leading to qualitatively different conformations relative to the well-studied classical worm-like chain.

We find that the ribbon can exist in three morphological phases as a function of the scaled tension, torque, and temperature (as shown in Fig. 4), which we characterize using the cumulative link, twist, and writhe densities. These phases, which correspond to HW, HT, and strongly disordered tangles, each have distinctive orientational correlation functions and thus should have clear experimental signatures. Interestingly, the transition between the HW and HT phases is continuous and similar to the spontaneous symmetry-breaking phase transition in magnetic systems (Fig. 3*F*), except that, here, the order parameter is a topological quantity, the link $\langle$Lk$\rangle$, that changes as a function of the applied torque. Furthermore, we note that, in the HW phase (seen in the limit of small applied torques), the local chirality keeps flipping due to the existence of multiple perversions, which are chirality-reversing localized defects, resulting in small $\langle$Lk$\rangle$. On the other hand, in the HT phase, the handedness of the ribbon persists over a long length scale, with few perversions, resulting in large $\langle$Lk$\rangle$. These observations lead to a rich morphological phase diagram for the loaded ribbon that should be amenable to experimental tests. This is in sharp contrast with the loaded worm-like chain, which exhibits either a randomly coiled or an elongated state in the absence of self-interaction terms in the free energy; complex morphologies such as plectonemes and solenoids are a consequence of excluded-volume interactions. Our study has uncovered the subtle interplay between topology, geometry, and statistical mechanics in a minimal setting for a naturally flat ribbon, with experimentally testable predictions. Extensions of the model to account for nonflat natural states (15) and excluded-volume interactions (49) as well as local order–disorder transitions induced by forces or torques (16) might be relevant for understanding morphological transitions in ribbon-like complex biological macromolecular assemblies.

Materials and Methods

Monte Carlo Simulations of Thermal Ribbons. We use Monte Carlo–based computational methods to study the equilibrium statistics and topology of a microscopic ribbon loaded by forces and torques, as detailed in *SI Appendix*. The simulations provide additional analysis of the fluctuating ribbon, including the role of finite-size effects and boundaries on the nature of the correlation functions between the different geometrical and topological quantities such as curvature, torsion, link, twist, writhe, etc.; a scaling analysis of the persistence length and wavenumber derived from the geometrical correlation functions; detection of perversions along ribbon; details of the topological analysis; and fitting the force–extension curve to analytic expressions.

Data Availability. All study data are included in the article and/or *SI Appendix*.

ACKNOWLEDGMENTS. E.H.Y. and F.D. acknowledge support from Nanyang Technological University, Singapore, under its Start Up Grant Scheme (04INS000175C230). The computational work for this article was performed on resources of the National Supercomputing Centre, Singapore (https://www.nscc.sg). L.G. is supported by the European Union via the ERC-CoG Grant HexaTissue and by Netherlands Organization for Scientific Research (Ministry of Education, Culture & Science), as part of the Vidi scheme. L.M. thanks the NSF Harvard MRSEC DMR 2011754, NSF EFRI 1830901, the Simons Foundation, and the Henri Seydoux Fund for partial financial support.

1. R. Phillips, J. Kondev, J. Theriot, H. Garcia, *Physical Biology of the Cell* (Garland Science, ed. 2, 2012).
2. P. G. de Gennes, *Scaling Concepts in Polymer Physics* (Cornell University Press, ed. 1, 1979).
3. M. Rubinstein, R. H. Colby, *Polymer Physics* (Oxford University Press, ed. 1, 2003).
4. C. Bustamante, J. F. Marko, E. D. Siggia, S. Smith, Entropic elasticity of lambda-phage DNA. *Science* **265**, 1599–1600 (1994).
5. C. Bustamante, Z. Bryant, S. B. Smith, Ten years of tension: Single-molecule DNA mechanics. *Nature* **421**, 423–427 (2003).
6. T. R. Strick, J. F. Allemand, D. Bensimon, A. Bensimon, V. Croquette, The elasticity of a single supercoiled DNA molecule. *Science* **271**, 1835–1837 (1996).
7. O. Kratky, G. Porod, Röntgenuntersuchung gelöster Fadenmoleküle [in German]. *Recl. Trav. Chim. Pays Bas* **68**, 1106–1123 (1949).
8. J. F. Marko, E. D. Siggia, Stretching DNA. *Macromolecules* **28**, 8759–8770 (1995).
9. J. F. Marko, E. D. Siggia, Statistical mechanics of supercoiled DNA. *Phys. Rev. E Stat. Phys. Plasmas Fluids Relat. Interdiscip. Topics* **52**, 2912–2938 (1995).
10. A. Marantan, L. Mahadevan, Mechanics and statistics of the worm-like chain. *Am. J. Phys.* **86**, 86–94 (2018).
11. A. V. Vologodskii, J. F. Marko, Extension of torsionally stressed DNA by external force. *Biophys. J.* **73**, 123–132 (1997).

12. J. F. Marko, Torque and dynamics of linking number relaxation in stretched supercoiled DNA. *Phys. Rev. E Stat. Nonlin. Soft Matter Phys.* **76**, 021926 (2007).
13. J. D. Moroz, P. Nelson, Torsional directed walks, entropic elasticity, and DNA twist stiffness. *Proc. Natl. Acad. Sci. U.S.A.* **94**, 14418–14422 (1997).
14. J. D. Moroz, P. Nelson, Entropic elasticity of twist-storing polymers. *Macromolecules* **31**, 6333–6347 (1998).
15. S. Panyukov, Y. Rabin, Thermal fluctuations of elastic filaments with spontaneous curvature and torsion. *Phys. Rev. Lett.* **85**, 2404–2407 (2000).
16. B. Chakrabarti, A. J. Levine, Nonlinear elasticity of an α-helical polypeptide. *Phys. Rev. E Stat. Nonlin. Soft Matter Phys.* **71**, 031905 (2005).
17. S. Yang *et al.*, Bottom-up approach toward single-crystalline VO_2-graphene ribbons as cathodes for ultrafast lithium storage. *Nano Lett.* **13**, 1596–1601 (2013).
18. M. Wang *et al.*, Nanoribbons self-assembled from short peptides demonstrate the formation of polar zippers between β-sheets. *Nat. Commun.* **9**, 5118 (2018).
19. G. J. Brouhard, L. M. Rice, Microtubule dynamics: An interplay of biochemistry and mechanics. *Nat. Rev. Mol. Cell Biol.* **19**, 451–463 (2018).
20. M. Dogterom, G. H. Koenderink, Actin-microtubule crosstalk in cell biology. *Nat. Rev. Mol. Cell Biol.* **20**, 38–54 (2019).
21. S. Zhang *et al.*, Coexistence of ribbon and helical fibrils originating from $hIAPP_{20-29}$ revealed by quantitative nanomechanical atomic force microscopy. *Proc. Natl. Acad. Sci. U.S.A.* **110**, 2798–2803 (2013).
22. B. K. Ho, P. M. Curmi, Twist and shear in β-sheets and β-ribbons. *J. Mol. Biol.* **317**, 291–308 (2002).
23. R. Everaers, R. Bundschuh, K. Kremer, Fluctuations and stiffness of double-stranded polymers: Railway-track model. *Eur. Lett.* **29**, 263–268 (1995).
24. T. Liverpool, R. Golestanian, K. Kremer, Statistical mechanics of double-stranded semiflexible polymers. *Phys. Rev. Lett.* **80**, 405–408 (1998).
25. R. Golestanian, T. B. Liverpool, Statistical mechanics of semiflexible ribbon polymers. *Phys. Rev. E Stat. Phys. Plasmas Fluids Relat. Interdiscip. Topics* **62**, 5488–5499 (2000).
26. M. Sadowsky, Ein elementarer Beweis für die Existenz eines abwickelbaren Möbiusschen Bandes und die Zurückführung des geometrischen Problems auf ein Variationsproblem [in German]. *Sitzungsber. Preuss. Akad. Wiss. Phys.-Math. Kl.* **22**, 412–415 (1930).
27. W. Wunderlich, Über ein abwickelbares Möbiusband [in German]. *Monatsh Math.* **66**, 276–289 (1962).
28. A. E. H. Love, *A Treatise on the Mathematical Theory of Elasticity* (Dover, New York, ed. 4, 1944).
29. J. H. White, Self-linking and the Gauss integral in higher dimensions. *Am. J. Math.* **91**, 693–728 (1969).
30. L. Mahadevan, J. Keller, The shape of a möbius band. *Proc. R. Soc. Lond. A* **1440**, 149–162 (1993).
31. E. L. Starostin, G. H. M. van der Heijden, Tension-induced multistability in inextensible helical ribbons. *Phys. Rev. Lett.* **101**, 084301 (2008).
32. B. Audoly, S. Neukirch, A one-dimensional model for elastic ribbons: A little stretching makes a big difference. *J. Mech. Phys. Solids* **153**, 104457 (2021).
33. L. Giomi, L. Mahadevan, Statistical mechanics of developable ribbons. *Phys. Rev. Lett.* **104**, 238104 (2010).
34. F. B. Fuller, The writhing number of a space curve. *Proc. Natl. Acad. Sci. U.S.A.* **68**, 815–819 (1971).
35. F. B. Fuller, Decomposition of the linking number of a closed ribbon: A problem from molecular biology. *Proc. Natl. Acad. Sci. U.S.A.* **75**, 3557–3561 (1978).
36. L. Freddi, P. Hornung, M. G. Mora, R. Paroni, A corrected Sadowsky functional for inextensible elastic ribbons. *J. Elast.* **123**, 125–136 (2016).
37. N. O. Kirby, E. Fried, Gamma-limit of a model for the elastic energy of an inextensible ribbon. *J. Elast.* **119**, 35–47 (2015).
38. N. Charles, M. Gazzola, L. Mahadevan, Topology, geometry, and mechanics of strongly stretched and twisted filaments: Solenoids, plectonemes, and artificial muscle fibers. *Phys. Rev. Lett.* **123**, 208003 (2019).
39. J. R. Quine, T. A. Cross, M. S. Chapman, R. Bertram, Mathematical aspects of protein structure determination with NMR orientational restraints. *Bull. Math. Biol.* **66**, 1705–1730 (2004).
40. K. Klenin, J. Langowski, Computation of writhe in modeling of supercoiled DNA. *Biopolymers* **54**, 307–317 (2000).
41. J. Marko, S. Coco, The micromechanics of DNA. *Phys. World* **16**, 37–41 (2003).
42. H. Zhou, Y. Zhang, Z. Ou-Yang, Elastic property of single double-stranded DNA molecules: Theoretical study and comparison with experiments. *Phys. Rev. E Stat. Phys. Plasmas Fluids Relat. Interdiscip. Topics* **62**, 1045–1058 (2000).
43. J. P. Sethna, *Statistical Mechanics: Entropy, Order, Parameters and Complexity* (Oxford University Press, ed. 2, 2021).
44. L. Tubiana, E. Orlandini, C. Micheletti, Probing the entanglement and locating knots in ring polymers: A comparative study of different arc closure schemes. *Prog. Theor. Phys. Suppl.* **191**, 192–204 (2011).
45. M. D. Frank-Kamenetskii, A. V. Lukashin, A. V. Vologodskii, Statistical mechanics and topology of polymer chains. *Nature* **258**, 398–402 (1975).
46. J. B. Keller, Tendril shape and lichen growth. *Lect. Math Life Sci.* **13**, 257–274 (1980).
47. F. Darwin, C. Darwin, *The Power of Movement in Plants* (Nabu, ed. 1, 2013).
48. S. J. Gerbode, J. R. Puzey, A. G. McCormick, L. Mahadevan, How the cucumber tendril coils and overwinds. *Science* **337**, 1087–1091 (2012).
49. D. Marenduzzo *et al.*, DNA–DNA interactions in bacteriophage capsids are responsible for the observed DNA knotting. *Proc. Natl. Acad. Sci. U.S.A.* **106**, 22269–22274 (2009).